Numerical Investigation of the Effect of Capsule Half-Cone Angle on a Supersonic Parachute System

Xiao-peng Xue [1]; Yusuke Nishiyama[2]; Yoshiaki Nakamura[3]; Koichi Mori[4]; Chih-Yung Wen[5]

Abstract

In this paper, the effects of the capsule half-cone angle on the dynamics of supersonic parachute systems are

[1] Currently Assistant Professor, School of Aeronautics and Astronautics, Central South University, Chang Sha, China 410083. E-mail: watt0304@hotmail.com.

[2] Currently AISIN AW CO., LTD., 10, Takane, Fujii-cho, Anjo, Aichi 444-1192, Japan. E-mail: yusuke.nishiyama1614@gmail.com.

[3] Currently Professor, Department of Mechanical Engineering, CHUBU University, 1200 Matsumoto-cho, Kasugai, Aichi 487-8501, JAPAN. E-mail: yoshi_nakamura@isc.chubu.ac.jp.

[4] Currently Associate Professor, Department of Aerospace Engineering, Nagoya University, 1 Furo-cho, Chikusa, Nagoya, Aichi 464-8603, JAPAN. E-mail: mori@nuae.nagoya-u.ac.jp.

[5] Currently Professor, Department of Mechanical Engineering, 6/F, FG Core, The Hong Kong Polytechnic University, Hung Hom, Kowloon, Hong Kong (Corresponding author) , Tel: +852 27666644; E-mail: cywen@polyu.edu.hk.

investigated. The supersonic flow over three-dimensional rigid parachute models are studied by numerically solving compressible Navier-Stokes equations. In this study, the parachute system has a capsule and a canopy. The cases with different capsule half-cone angle are carried out. The computational results show unsteady pulsating flow fields exit in all the cases and are in reasonable agreement with the experimental data. The results also show that the capsule wake/canopy shock interaction causes a significantly higher pressure around the parachute system in comparison to the capsule shock/canopy shock interaction, thus providing the primary source of the unsteadiness in the flow field. As the capsule half-cone angle (θ) is increased, the difference in the pressure distribution inside the canopy also increases, and the wake/shock interaction plays a more significant role in the unsteady flow mode. Moreover, when θ is increased, this results in weaker aerodynamic interactions, including the wake/shock and shock/shock interactions, which is favorable for a supersonic parachute system.

Introduction

In the Mars mission, the supersonic parachute played a very important role in the entry, descent, and landing of the Mars rover (Cruz et al., 2006). To date, many researchers have studied the effects of the complex aerodynamic interactions on the performance of supersonic parachutes. Lingard et al. (2005; 2007) carried out early simulations on ~~the~~ flexible parachute systems at supersonic conditions, and found that there is aerodynamic interference between the capsule wake and the canopy shock as a function of Mach number and the trailing distance. Recently, subscale models of Mars Science Laboratory (MSL) parachutes were experimentally and numerically investigated. The studies found that the flow instability is derived from aerodynamic interference due to the interaction of the capsule wake with the canopy shock, which depends on the Mach number, Reynolds number, capsule shape and proximity to the capsule (see Sengupta and Kelsch et al. 2009; Sengupta and Steltzner el al. 2009; Sengupta 2011). Furthermore, Barnhardt et al. (2007) used the detached eddy simulation (DES) method on a rigid parachute model to investigate the effects of wake/shock interaction and the corresponding flow instabilities. They illustrated that the time-dependent deficit in the capsule wake interacts with the canopy shock, which causes unsteadiness in the flow around the parachute. Gidzak et al. (2008; 2009) also used the DES method to further investigate both rigid and flexible parachutes and compared their data with those obtained from wind tunnel tests. They found that the time scale for the canopy-scale motions is longer than that of the variations in the canopy drag. To fully understand the complexity of the unsteady flow field around a supersonic parachute, the current research group have carried out numerical and experimental parametric studies on the parachute dynamics since 2013. The authors have numerically simulated a rigid parachute with a rather short trailing distance (X/d = 2.38), and found that there is an unsteady pulsating flow field around the parachute (Xue et al., 2013). Nishiyama (2013) and Xue et al. (Xue et al., "High-Speed Unsteady Flow Pasts Two-Body Configurations," submitted; "Parametric Study on Aerodynamic Interaction of a Supersonic Parachute System," submitted, Nagoya University, Nagoya, Japan) further experimentally and numerically investigated the effects of the trailing distance (X/d) and the ratio of the capsule diameter to the canopy diameter (d/D) on parachute performance at supersonic conditions. Four unsteady flow modes were found according to the variations in the flow field under the effect of *X/d*, which are: ① pulsation mode, ② oscillation mode, ③ transition from ② to ④, and ④ narrow wake/rear shock interaction. As *d/D* increases, the variation in the flow mode becomes more sensitive and changes quickly under the impact of *X/d*, and the ranges of the pulsation and oscillation modes are reduced. As a result, in seeking to improve the parachute performance, a large *d/D* value is advised. In addition, the effects of the suspension lines on the flow field around supersonic rigid parachute have been investigated by using a simple "immersed boundary technique" (Xue et al. 2015). It ~~could be~~ observed that ~~the shock to~~ the suspension line generated ~~onto it causes visible density disturbances,~~ which interfere with the canopy bow-shock and exacerbate the flow field instability around the parachute system.

Therefore, to further investigate ways to suppress the aerodynamic interactions between the capsule and the canopy, the role of the capsule half-cone angle is examined in this paper. Numerical simulations of the flows around the capsules with different half-cone angles, θ, are conducted to investigate ~~the~~ effect ~~of θ~~ on the flow instability at a freestream Mach number of 2. The computational results are then compared with the experimental data measured at the Institute of Space and Astronautical Science (ISAS)/Japan Aerospace Exploration Agency (JAXA).

Parachute Models

In this study, the supersonic parachute system consists of a capsule and a canopy that is connected by a rod. As shown in Fig. 1, the canopy is ~~a~~ hemispherical in shape with an outer diameter of D and a thickness of h. The diameter of the frontal surface of the capsule is d. The capsule is ~~a~~ conical in shape ~~form~~ with a half-cone angle of θ. X is the axial distance from the frontal surface of the capsule to the inlet of the canopy, X/d the trailing distance of the parachute, and d/D the ratio of the diameter of the capsule to the diameter of the canopy. This configuration is the same as the model used in the experiments. The capsule and the canopy are connected with a connecting rod and the entire parachute model is supported with a thicker rod from the top of the canopy to the wind tunnel system. Note that the effects of the connecting rod between the capsule and canopy have been investigated in ~~the~~ earlier study by Xue et al. (2013). It was found that except for the minor differences in the shock shape caused by the connecting rod, the effects of the connecting rod on the flow field and pressure distribution on the body surfaces are rather minimal, and the pulsation mechanism ~~in the case without a connecting rod~~ is identical ~~to that for the case in which a connecting rod is used~~.

As shown in Table 1, the effects of different half-cone angle, θ, on the flow instability are investigated. Here, the length of the capsule (X_1) and the diameter of the rear surface of the capsule (the diameter of the connecting rod, d_1) are fixed. When θ changes, X/d and d/D both change correspondingly, which significantly affect the stability of the flow field (Nishiyama 2013; Xue et al., "High-Speed Unsteady Flow Pasts Two-Body Configurations," submitted; Xue et al., "Parametric Study on Aerodynamic Interaction of a Supersonic Parachute System," submitted, Nagoya University, Nagoya, Japan).

Computational Conditions and Methods

Computational Conditions

The freestream conditions used in the simulations in this study are set in accordance with those in the experiments by Nishiyama (2013), and shown in Table 2.

Numerical Methods

The calculations were performed by using an in-house single-block structured code ~~that is parallelized~~, where 3D compressible Navier-Stokes equations are solved to simulate the supersonic flow field around a parachute system. The inviscid fluxes were evaluated using the Simple High-resolution Upwind scheme (SHUS) (Shima 1996), and its accuracy was improved by means of the 3rd-order MUSCL scheme (Van Leer 1977) combined with the Van Albada flux limiter (Anderson 1986). The viscous terms were computed by using ~~the~~ 2nd-order central differencing scheme. The coefficient of viscosity was computed with Sutherland's law. In addition, to ensure the time accuracy of the numerical results, time advancement was performed using ~~the~~ 3rd-order total variation diminishing Runge-Kutta scheme (Shu 1988). The dimensionless time step was set as 1.0×10^{-5} in all of the cases, to limit the Courant-Friedrichs-Lewy number to about 0.5. Finally, at the inflow boundary, all conservative variables were determined by the freestream values, as shown in Table 2. At the outer boundary, the conservative variables were solved from the solution inside the computational domain (zero gradient condition). For the solid body, the no-slip and adiabatic conditions were applied to treat the boundary surfaces.

Note that a turbulence model was not employed in this study, because previous studies that used a rigid parachute model demonstrated a satisfactory agreement between the results obtained by laminar numerical simulations and those experimentally obtained (Xue et al. 2013). Consequently, an extended form of the numerical code employed in Xue et al. (2013) is used for the simulations in this study. Numerical simulations combined with the DES method will also be conducted to investigate the complicated mechanism of an unsteady flow field around a parachute in the near future.

Grids

The flow field around a 3D rigid parachute model was simulated by using a structured, single-block grid. Note that the grid created involves a meridional plane, due to the axisymmetric configuration of the parachute system. The 3D view of the grid of the parachute mode for Case B is shown in Fig. 1(b) and the validity test of the grid convergence was demonstrated in the previous study (Xue et al. 2013). Thus, in this study, all of the simulations are performed using a similar grid with the same grid number of 3,387,664 and the same cell number of 3,293,136 for all three cases. The minimum grid size (cell height) is 0.08 mm for the cells adjacent to the wall surface.

Validation of the Numerical Methods

In the authors' previous study (Xue et al., "High-Speed Unsteady Flow Pasts Two-Body Configurations," submitted, Nagoya University, Nagoya, Japan), the validity of the numerical method was evaluated by comparing the simulation results obtained in Case B (θ = 20 deg) for the time-resolved pressure at point Q on the inner surface of the canopy (see Fig. 1(a)) with the results measured by using a high-frequency pressure transducer (Kulite™ XT-190-200A) at the ISAS/JAXA (Nishiyama 2013). Moreover, the representative experimental and numerical instantaneous flow fields also show reasonable agreement. Thus the validation of the numerical method is ~~basically~~ ~~confirmed,~~

Results and Discussion

In the authors' previous study (Xue et al., "Parametric Study on Aerodynamic Interaction of a Supersonic Parachute System," submitted, Nagoya University, Nagoya, Japan), it was found that there are four modes according to the variations in the flow field under the effect of the trailing distance (*X/d*) and the ratio of the diameter of the capsule to the canopy (*d/D*), including ①: pulsation mode, ②: oscillation mode, ③: transition from ② to ④, and ④: narrow wake/rear shock interaction. The quantified effects were summarized in the referenced paper. When *d/D* is equal to 0.2, *X/d* is ~~less than~~ approximately 5.8, and the unsteady flow around the parachute exhibits ~~the~~ pulsation mode (Xue et al. 2013). As *d*/*D* increases, the variation in the flow mode ~~becomes sensitive~~ and changes quickly under the impact of *X*/*d*. The critical values and range of *X*/*d* for the transition of the unsteady flow mode become smaller. When *d*/*D* is increased to 0.33, the flow ~~mode~~ becomes ~~the~~ pulsation mode as long as *X/d* is less than approximately 2.8. As shown in Table 1, as θ is increased from10 to 30 deg, the *d/D* for cases A-C increases from 0.15 to 0.26, and *X/d* for cases A-C decreases from 5.06 to 2.89. Thus, the flow field around the parachute shows ~~the~~ pulsation mode for all three cases, where a hemispherical shaped shock wave is formed in front of the capsule, which inflates and moves outward in the radial direction. Notably, this phenomenon is consistent with the pulsation flows reported in the literatures (Feszty et al. 2004; Panaras et al. 2009, Xue et al. 2013), and it is caused by upstream propagation and lateral expansion of the interaction of the capsule wake/canopy shock and capsule shock/canopy shock, which has been investigated in detail in the authors' earlier study (Xue et al. 2013).

As shown in Fig. 2, the ratios of the stand-off distance of capsule shock, Δ, to the distance between the capsule and the canopy, *X*=90mm, for Cases A, B and C are plotted to verify the pulsation flow mode. In Fig. 2, t_1 is the non-dimensional time, and is defined as $t_1 = t * V_\infty / D$ (Feszty et al. 2004; Xue et al. 2013). It can be seen that there is a significant vibration in the stand-off distance for all the cases, which clearly shows that the pulsation mode characterizes the flow, and the capsule shock (foreshock) periodically moves upstream and downstream with time. The fluctuation amplitude gradually decreases as θ is increased. Moreover, as θ is decreased, the foreshock formed ahead of the capsule stays closer to the capsule surface, and its greater fluctuation in the stand-off distance leads to instability of the flow field around the capsule.

In addition, it can be seen from Fig. 2 that as θ is decreased, the time period of the pulsation mode becomes longer. Figure 3 shows the comparison of the experimental and CFD Strouhal numbers, *St*, under different capsule half-cone angle, θ. The Strouhal number of the pulsation mode, which describes the frequency of the flow oscillations (White 1999), is defined as follows:

$$St \equiv \frac{f \times D}{V_\infty} \tag{1}$$

where f is the oscillation frequency, D the canopy diameter, and V_∞ the freestream velocity. Here the experimental and CFD oscillation frequencies were extracted from the pressure data of point Q (see Figs. 1(a)) and the shock stand-off distance data in Fig. 2 via power spectrum analysis. Good agreement is observed. The differences between the computational *St* from the stand-off distance of the foreshock and the experimental *St* are 4 %, 0.4%, 1% for Cases A, B and C, respectively. *St* becomes larger as θ is increased (see the fit line in Fig. 3), which indicates that the frequency (time period) of the pulsation flow is increased (decreased). Moreover, the frequencies of the pressure change inside the canopy are consistent with those of the flow field ~~pulsating.~~

Figure 4 presents typical Mach number contours in two instantaneous flow fields for Cases A, B and C, with increases in θ from 10 to 30 deg, respectively. It can be observed that the aerodynamic interactions, that is, the capsule wake/canopy shock interaction (left) and the capsule shock/canopy shock interaction (right) occur in all the cases with the pulsation mode (Xue et al. 2013). When compared among the different θ cases, it can be found that as θ is decreased, the capsule wake is weakened, and when the canopy shock moves upstream, the coupling between the capsule wake and the canopy shock is also weakened, however, the distance between the capsule shock and canopy shock is reduced (see black ellipse on left side of Fig. 4). As a consequence of this effect, when θ is decreased, the capsule shock (S1) interacts with the canopy shock (S2) more intensively in the late stage of the pulsation mode (see right side of Fig. 4), and their coupling becomes longer and stronger. Furthermore, as θ is decreased, shear layer L1 separates from the capsule neck, and a stronger shock (S3) forms, especially at θ =10 deg, when stronger aerodynamic interactions moves laterally, and another shock S4 is generated. Meanwhile, it can be seen from the right side of Fig. 4 that, Cases A and B exhibit stronger coupling between the capsule shock (S1) and canopy shock (S2), and the interaction location (triple point) is closer to the symmetric axis of the parachute system (see double-headed arrows in Fig. 4), which leads to a greater pressure inside the canopy (see Fig. 5). Thus, as θ is decreased, the shock/shock interaction becomes stronger. In addition, as θ is increased, the stand-off distance of the shock ahead of the capsule (foreshock) becomes larger, which is consistent with the result in Fig. 2.

Moreover, it can be seen from Fig. 5 that, the capsule wake/canopy shock interaction leads to a significantly larger pressure around the parachute system than that of the capsule shock/canopy shock interaction, which provides ~~the~~ major source of the unsteadiness in the flow field for the pulsation mode here. In addition, as θ is increased, the difference in pressure distribution inside the canopy also increases, which means that the wake/shock interaction has a stronger effect on the unsteady flow mode.

In summary, when the distance between the capsule and canopy (X) and the diameter of the canopy (D) are fixed, as θ is increased, the aerodynamic wake/shock and shock/shock interactions are weakened and the locations of the interactions also move outside from the parachute system. Consequently the averaged pressure inside the canopy is reduced, as illustrated further in Fig. 6, where the maximum differences between the computational and experimental pressure are less than 8 %, 11%, 8% for Cases A, B and C, respectively. Therefore, a larger capsule half-cone angle (greater than 30 deg) suppresses the aerodynamic interactions between the capsule and canopy and is favorable for the supersonic parachute system.

Conclusions

In this study the supersonic flow over 3D rigid parachute models were numerically simulated at a freestream Mach number of 2. The effects of the capsule half-cone angle on the unsteady flow field around the parachute system and the parachute dynamics were examined. The results are summarized as follows:

- The computational results in all the cases show good agreement with the experimental data obtained from the experiments carried out at the JAXA. The unsteady flow 'pulsation mode' is observed for all the cases.
- In comparing the cases with different half-cone angles, θ, it can be observed that there is a significant variation in the stand-off distance of capsule shock. This illustrates clearly that the pulsation mode characterizes the flow, and the capsule shock periodically moves upstream and downstream with time. As θ is decreased, the capsule shock stays closer to the capsule frontal surface, and the greater fluctuation in the stand-off distance leads to instability of the flow field around the capsule.
- When the distance between the capsule and canopy (X) and the diameter of canopy (D) are fixed, as θ is increased, this results in weaker aerodynamic interactions, including the capsule wake/canopy shock and capsule shock/canopy shock interactions. Therefore, a larger capsule half-cone angle (greater than 30 deg) suppresses the aerodynamic interactions between the capsule and canopy and improves the unsteady flow field around the parachute system, which is favorable for the supersonic parachute system.
- As observed in Fig. 5, the capsule wake/canopy shock interaction leads to a significantly larger pressure around the parachute than that of the capsule shock/canopy shock interaction, thus providing the major

source of the unsteadiness in the flow field for the pulsation mode here. In addition, as θ is increased, the difference in the pressure distribution inside the canopy becomes greater, and the wake/shock interaction plays a larger role on the unsteady flow mode.

References

Anderson, W.K. Thomas, J.L. and Van Leer, B. (1986). “Comparison of Finite Volume Flux Vector Splitting for the Euler Equations,” AIAA Journal, 24(9),1453-1460.

Barnhardt, M., Drayna, T., Nompelis, I., Candler, G. V. and Garrard, W. (2007). “Detached Eddy Simulations of the MSL Parachute at Supersonic Conditions,” AIAA Paper 2007-2529.

Cruz, J.R. and Lingard, J., “Aerodynamic Decelerators for Planetary Exploration: Past, Present, and Future,” AIAA Paper 2006-6792, 2006.

Feszty, D., Badcock, K.J. and Richards, B.E.(2004). “Driving Mechanisms of High-Speed Unsteady Spiked Body Flows, Part 1: Pulsation Mode,” AIAA Journal, 42(1), 95-106.

Gidzak, V., Barnhardt, M., Drayna, T., Nompelis, I., Candler, G. V. and Garrard, W. (2008). “Simulation of Fluid-Structure Interaction of the Mars Science Laboratory Parachute,” AIAA Paper 2008-6910.

Gidzak, V., Barnhardt, M., Drayna, T., Nompelis, I., Candler, G. V. and Garrard, W. (2009). “Comparison of Fluid-Structure Interaction Simulation of the MSL Parachute with Wind Tunnel Tests,” AIAA Paper 2009-2971.

Kitamura, K., Men’shov, I., Nakamura, Y. (2005). “Shock/Shock and Shock/Boundary-Layer Interactions in

Two-Body Configurations," AIAA Paper 2005-4893.

Lingard, J. and Darley, M. (2005). "Simulation of Parachute Fluid Structure Interaction in Supersonic Flow," AIAA Paper 2005-1607.

Lingard, J., Darley, M. and Underwood, J.C.(2007). "Simulation of Mars Supersonic Parachute Performance and Dynamics," AIAA Paper 2007-2507.

Nishiyama,Y.(2013). "Aerodynamic Characteristics of the Supersonic Parachute with its Opening Process," Master thesis of Nagoya University.

Panaras, A.G., Drikakis, D. (2009). "High-speed Unsteady Flows Around Spiked-Blunt Bodies," Journal of Fluid Mechanics, 632, 69-96.

Sengupta, A. (2011). "Fluid Structure Interaction of Parachutes in Supersonic Planetary Entry," AIAA Paper 2011-2541.

Sengupta, A., Kelsch, R., Roeder, J. Wernet, M., Witkowaski, A. and Kandis, M. (2009). "Supersonic Performance of Disk-Gap-Band Parachutes Constrained to a 0-Degree Trim Angle," Journal of Spacecraft and Rockets, 46, 1155-1163.

Sengupta, A., Steltzner, A. Witkowski, A., Candler, G. and Pantano, C. (2009). "Findings from the Supersonic Qualification Program of the Mars Science Laboratory Parachute System," AIAA Paper 2009-2900.

Shima, E. and Jounouchi, T. (1996). "Roe of CFD in Aeronautical Engineering (No.14) -AUSM Type Upwind Schemes-, NAL-SP30," Proceedings of 13th NAL symposium on Aircraft Computational Aerodynamics, 41–46.

Shu, C.W. and Osher, S. (1988). “Efficient Implementation of Essentially Non-Oscillatory Shock-Capturing Schemes,” Journal of Computational Physics, 77(2), 439-471.

Van Leer, B. (1977). “Toward the Ultimate Conservative Difference Scheme. IV. A New Approach To Numerical Convection,” Journal of Computational Physics, 23(3), 276-299.

White, F.M. (1999). “Fluid Mechanics (4th ed),” McGraw Hill, 295-297.

Xue, X., Koyama, H. and Nakamura, Y. (2013). “Numerical Simulation on Supersonic Aerodynamic Interaction of A Parachute System,” Transactions of the Japan Society for Aeronautical and Space Sciences, Aerospace Technology Japan, 11, 33-42.

Xue, X., Koyama, H., Nakamura, Y. and Wen, C.Y., “Effects of Suspension Line on Flow Field Around a Supersonic Parachute,” Aerospace Science and Technology, Vol. 43, 2015, pp.63-70.

Fig. 1 (a): Parachute model used in the present computation and capsule geometry (dimensions are in the unit of mm); (b) 3D view of grid of parachute model for Case B in this study with the conditions on all the physical boundaries specified.

Fig. 1(a) No caption

Fig. 1(b) No caption

Fig. 2 Comparison of the ratios of the foreshock stand-off distance ahead of the capsule, Δ, to the distance

between the capsule and the canopy, *X*=90mm, for Cases A, B and C.

Fig. 3 Comparison of experimental and CFD Strouhal numbers for the effect of the capsule half-cone angle, θ. The line stands for the linear fit to the Strouhal number based on the CFD pressure variation at point Q.

Fig. 4 Typical Mach number contours in two instantaneous flow fields for Cases A, B and C with increases in θ from 10 to 30 deg, which show the flow features of the aerodynamic interactions: the capsule wake/canopy shock and the capsule shock/canopy shock interactions. Black ellipse marks the distance between the capsule shock and canopy shocks. The same scale with a black arrow is used to compare the triple-point positions in the three cases. S1 represents the capsule shock, S2 the canopy shock, S3 and S4 the shock waves, and L1 the shear layer.

Fig. 4 (a) θ =10 deg (left: 20/34T_{10}; right: 26/34T_{10})

Fig. 4 (b) **θ =20 deg (left: 19/32T_{20}; right: 25/32T_{20})**

Fig. 4(c) **θ =30 deg (left: 17/30T_{30}; right: 24/30T_{30})**

Fig. 5 Typical surface pressure contours in two instantaneous flow fields for Cases A, B and C with increases in θ from 10 to 30 deg in Fig. 4: the capsule wake/canopy shock interaction (left) and the capsule shock/canopy shock interaction (right).

Fig. 5 (a) θ =10 deg (left: 20/34T_{10}; right: 26/34T_{10})

Fig. 5 (b) **θ =20 deg (left: 19/32T_{20}; right: 25/32T_{20})**

Fig. 5(c) **θ =30 deg (left: 17/30T_{30}; right: 24/30T_{30})**

Fig. 6 Comparison of experimental and CFD averaged pressure distribution on the inner surface of the canopy for Cases (a) A, (b) B, (c) C. (d) is a summary of the pressure distribution data for all the cases.

Fig. 6(a) No caption

Fig. 6(b) No caption

Fig. 6(c) No caption

Fig. 6(d) No caption

Table 1 Specifications for the three cases in this study

Case	A	B	C
θ (deg)	10	20	30
d (mm)	17.8	24.0	31.1
d_1 (mm)	12	12	12
D (mm)	120	120	120
X (mm)	90	90	90
X_1 (mm)	16.5	16.5	16.5
d/D	0.15	0.2	0.26
X/d	5.06	3.75	2.89

Table 2 Flow conditions employed in the CFD simulations

M_∞	Re	P_0	P_∞	T_∞
2.0	$2.04\times10^7 m^{-1}$	160kPa	20.3kPa	165K

Fig.1(a)
Click here to download Figure: Fig.1(a).pdf

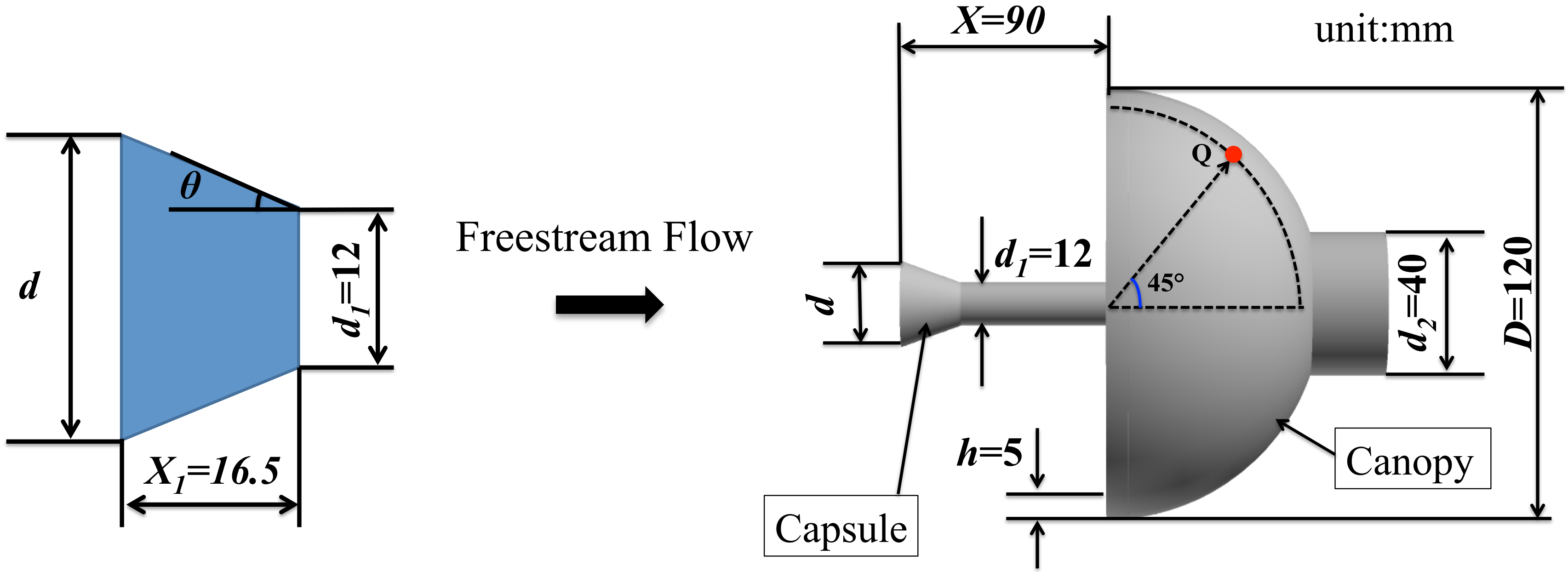

Fig.1(b)

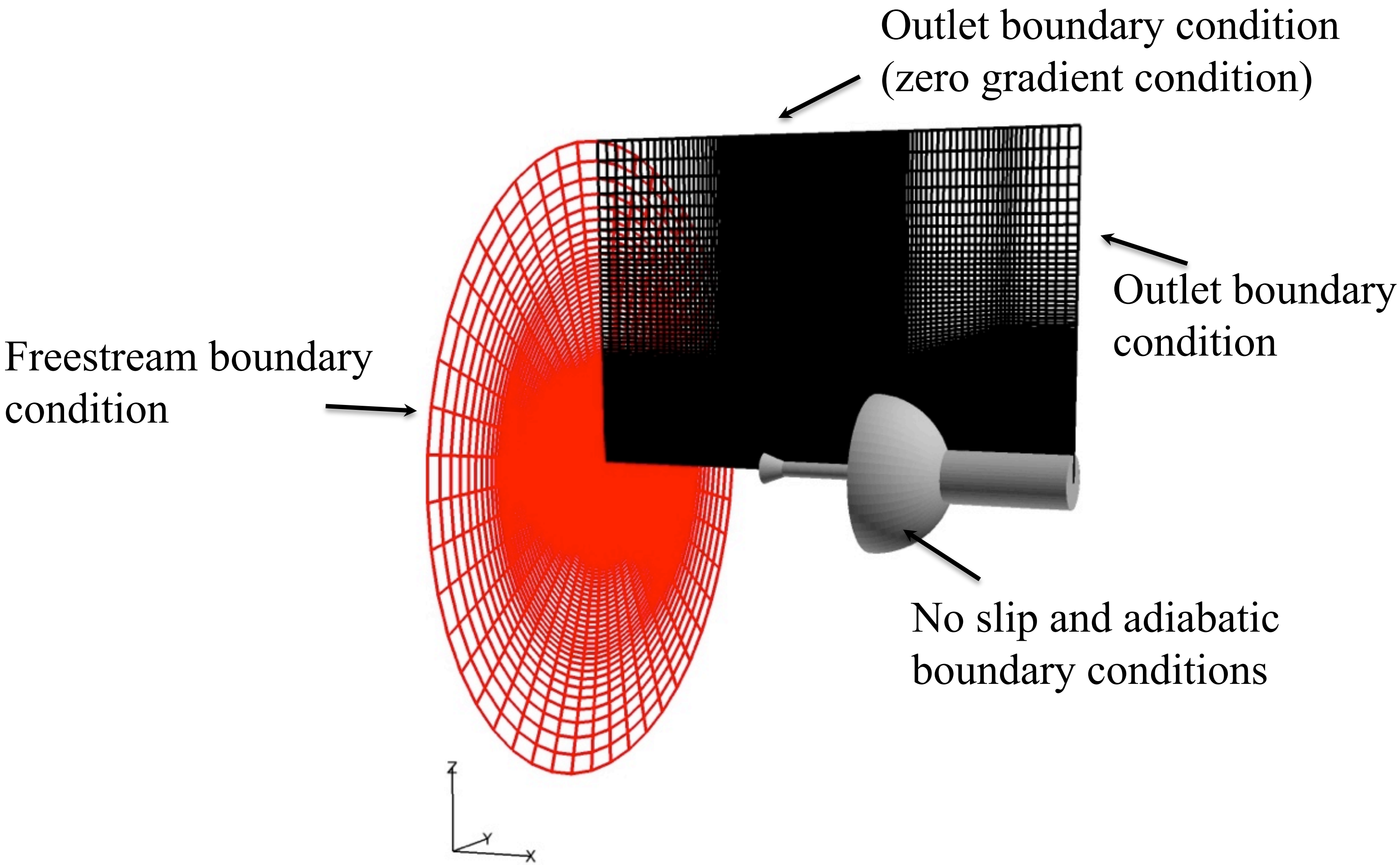
Outlet boundary condition
(zero gradient condition)
Outlet boundary
condition
Freestream boundary
condition
No slip and adiabatic
boundary conditions
z
y
x

Fig.2
Click here to download Figure: Fig.2.pdf

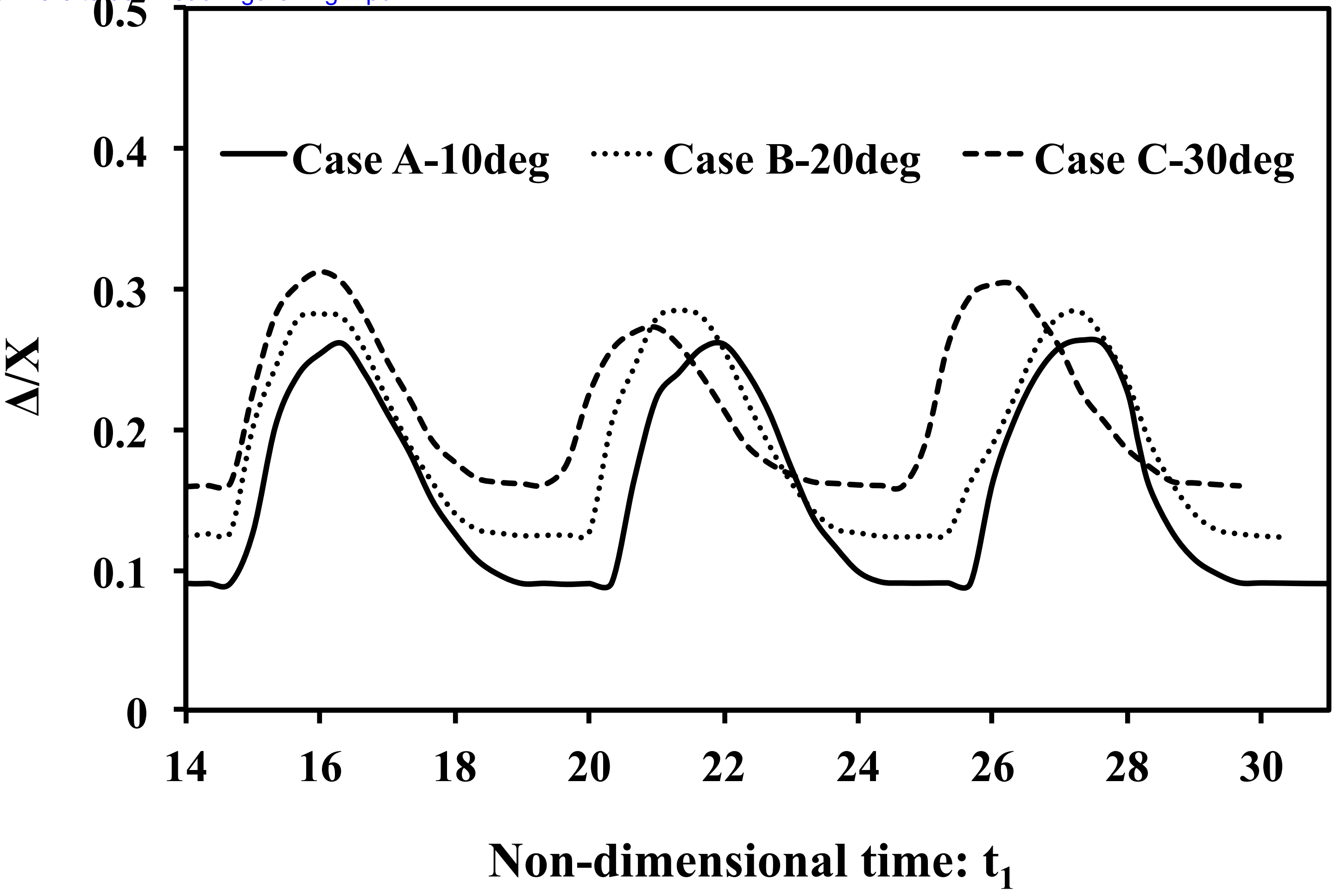

Fig.3

Click here to download Figure: Fig.3.pdf

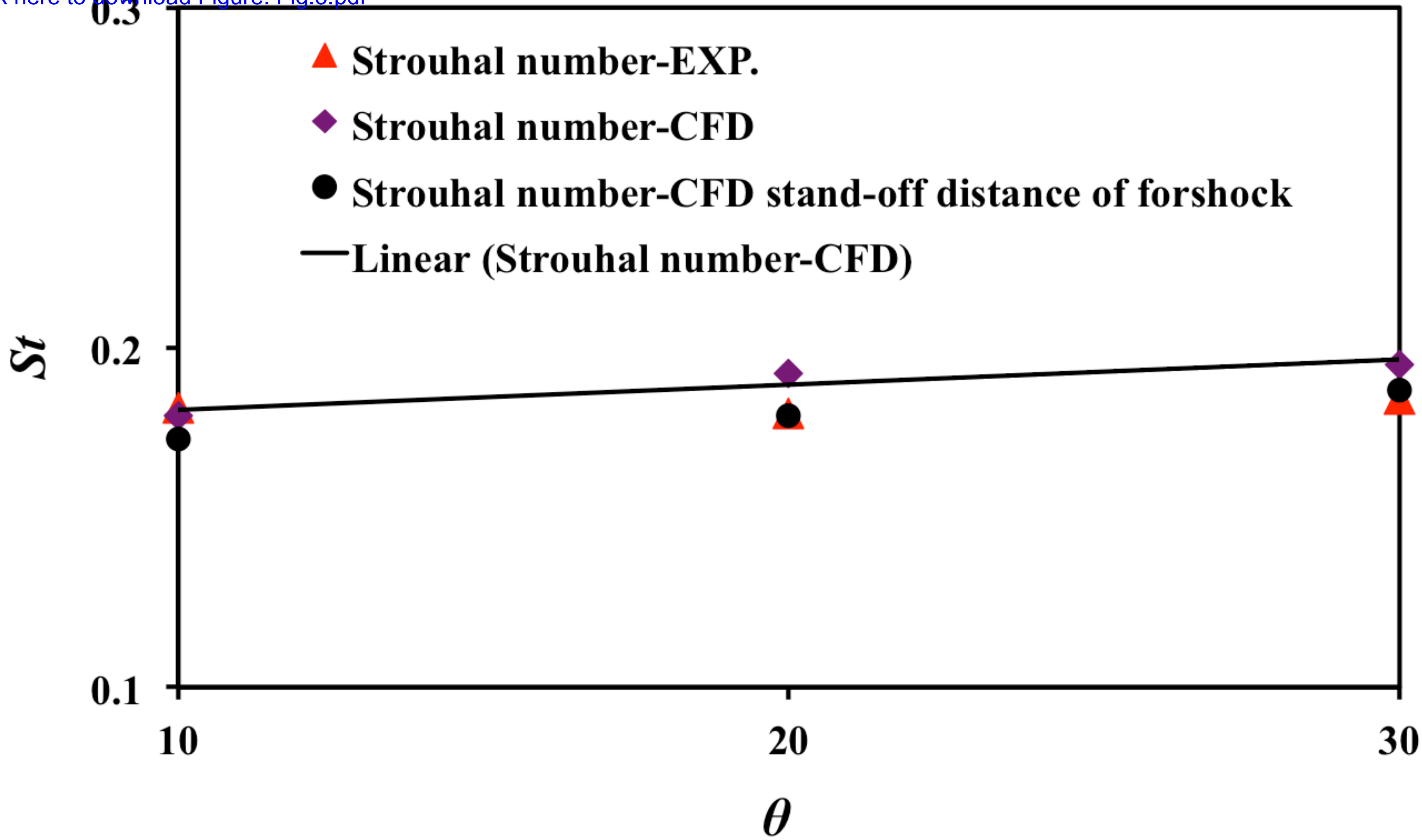

Fig.4(a)-Left

Click here to download Figure: Fig.4(a)-Left.pdf

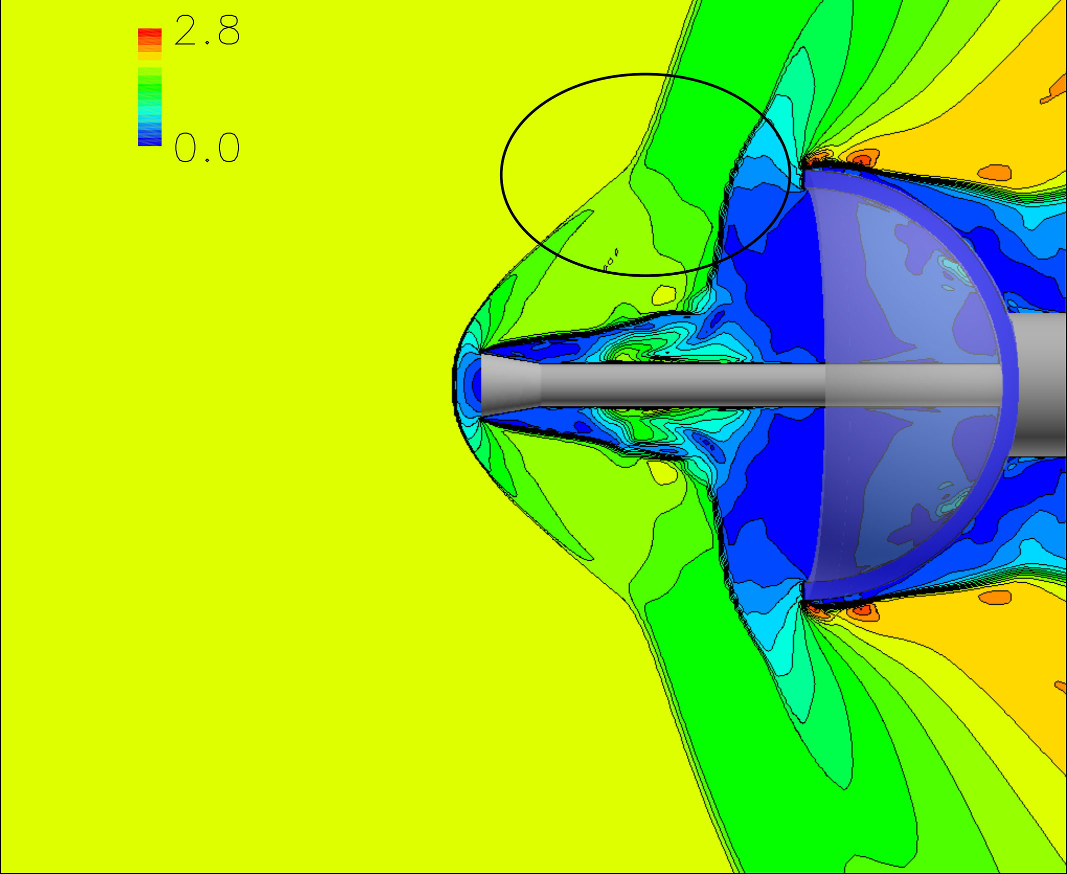

Fig.4(a)-Right

Click here to download Figure: Fig.4(a)-Right.pdf

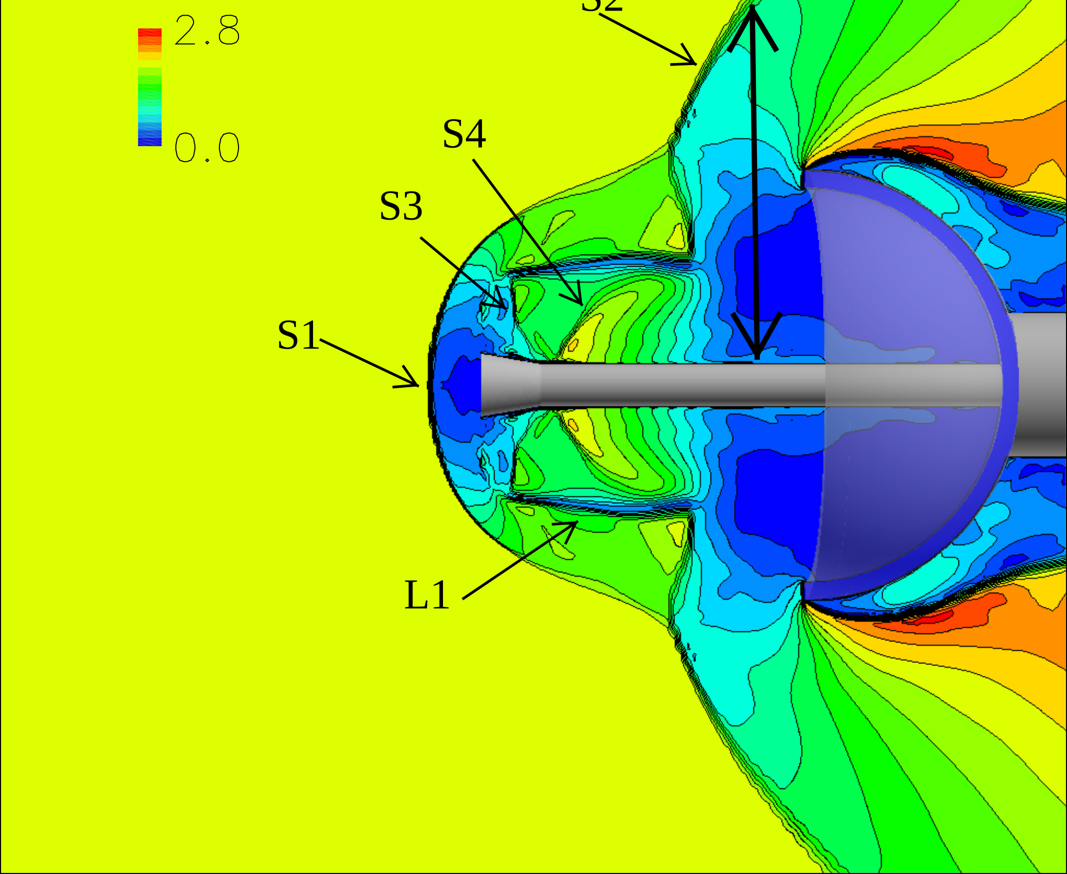

Fig.4(b)-Left

Click here to download Figure: Fig.4(b)-Left.pdf

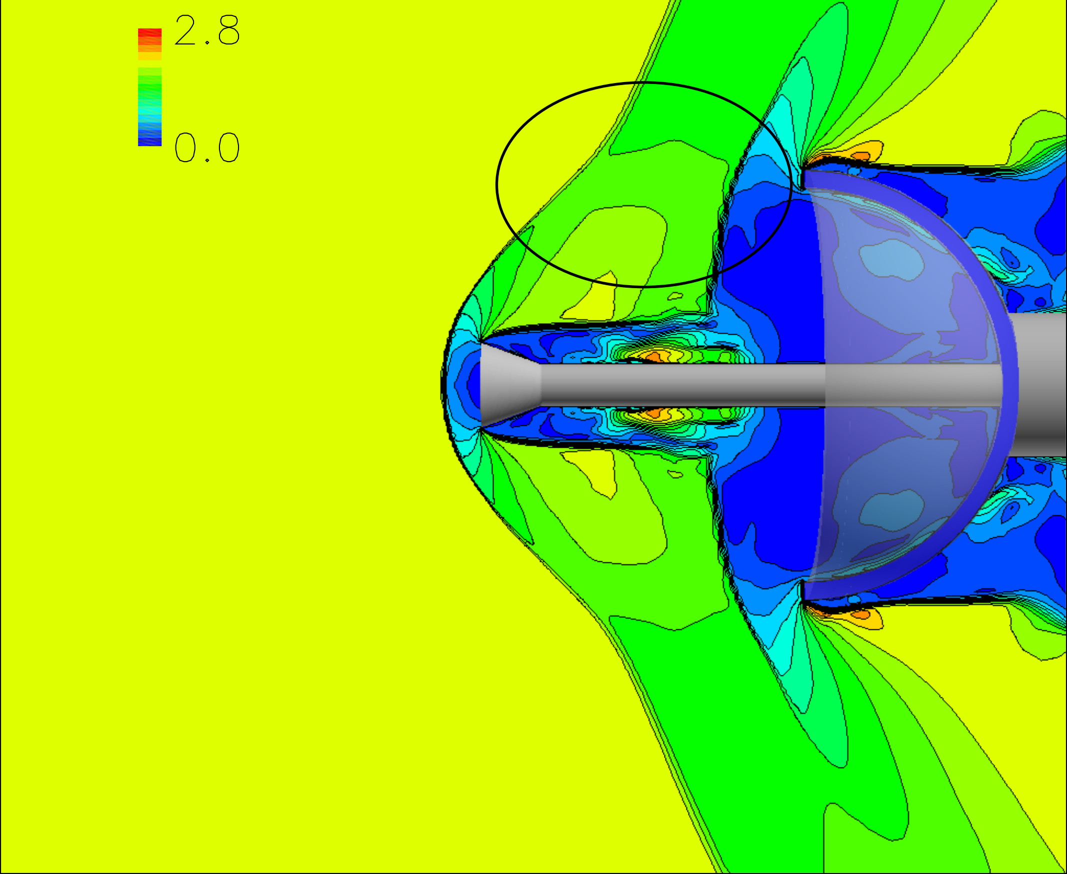

Fig.4(b)-Right

Click here to download Figure: Fig.4(b)-Right.pdf

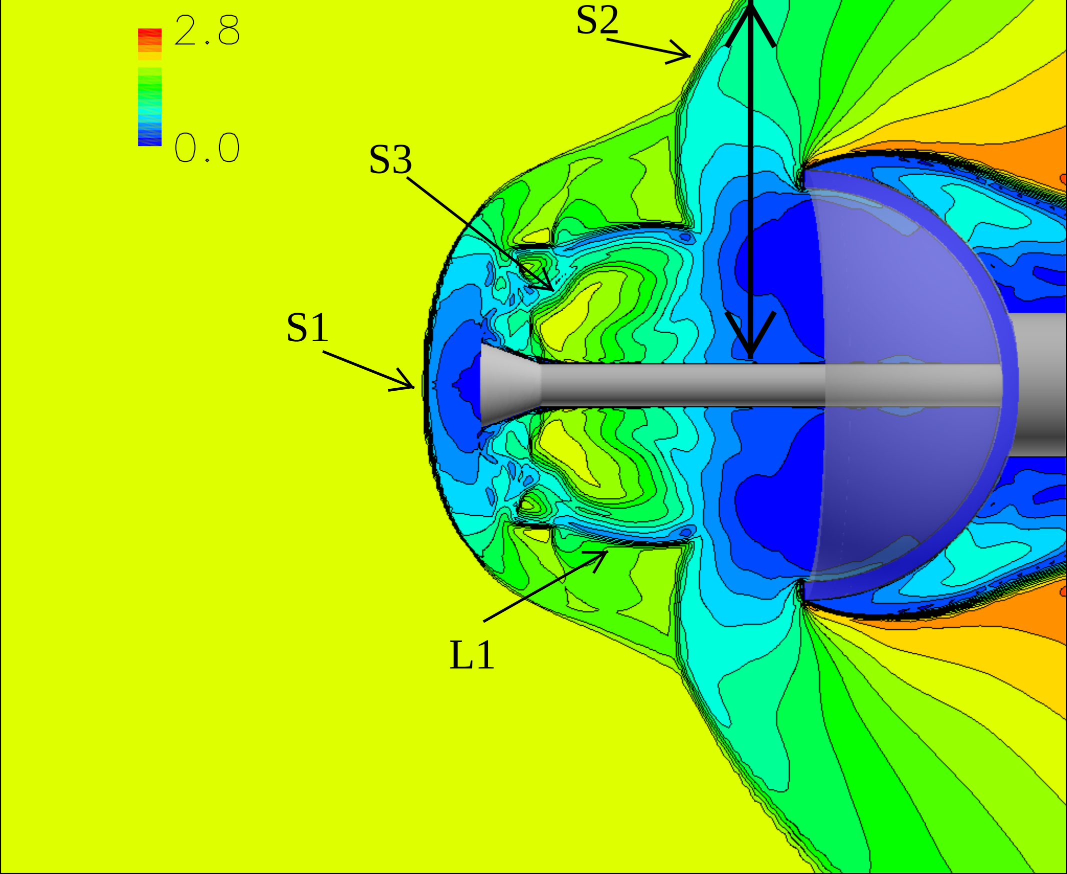

Fig.4(c)-Left

Click here to download Figure: Fig.4(c)-Left.pdf

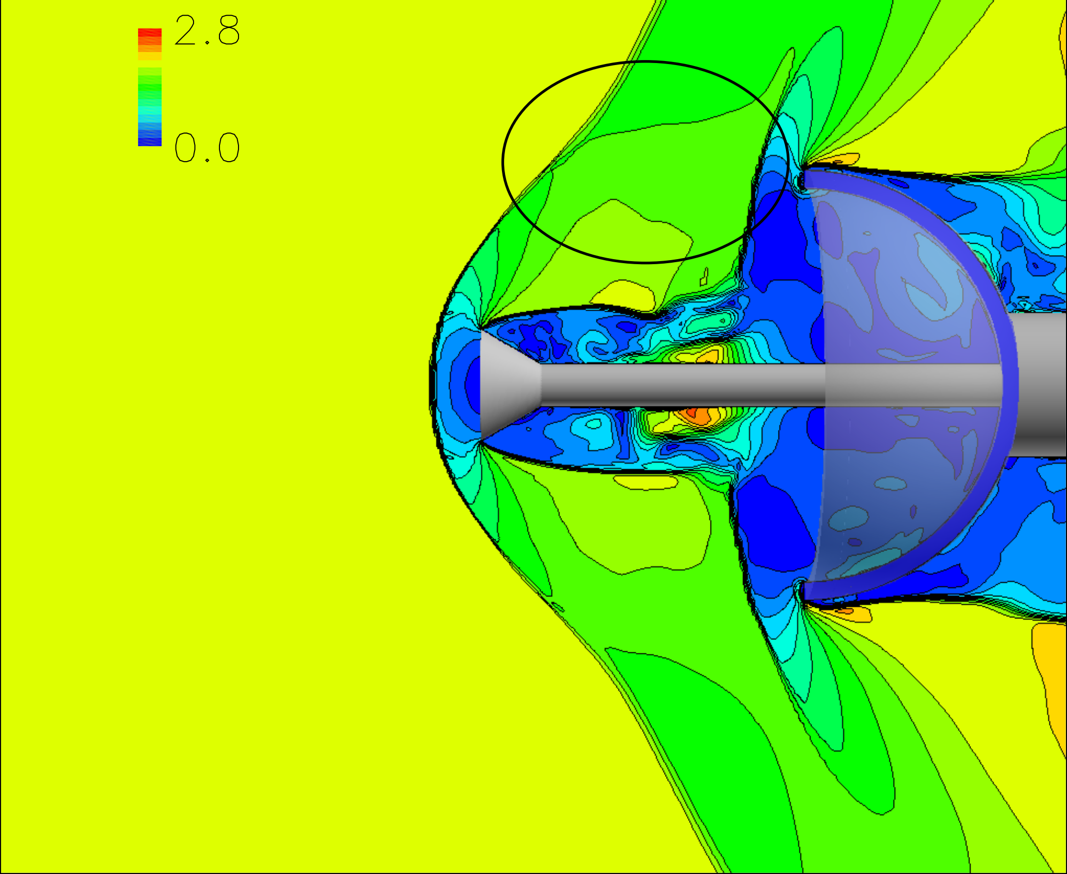

Fig.4(c)-Right

Click here to download Figure: Fig.4(c)-Right.pdf

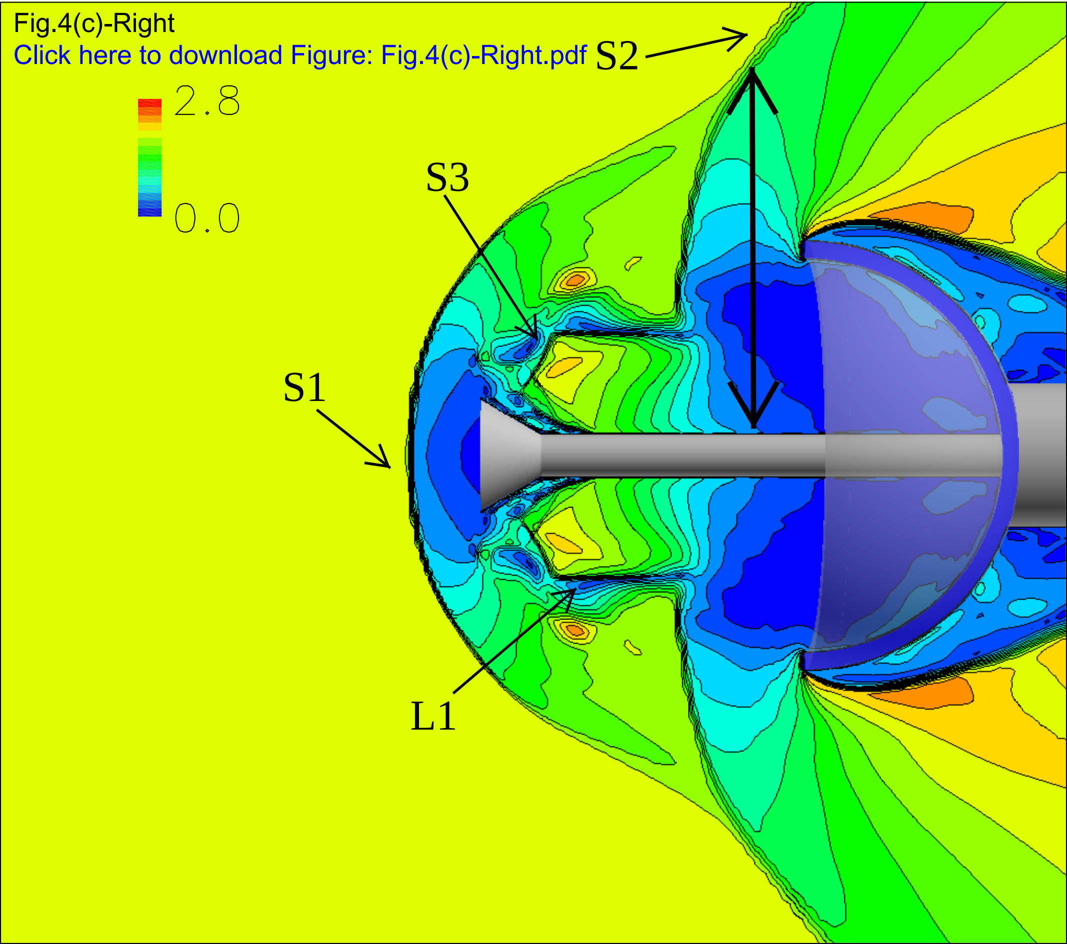

Fig.5(a)-Left
Click here to download Figure: Fig.5(a)-Left.eps

Fig.5(a)-Right
Click here to download Figure: Fig.5(a)-Right.eps

Fig.5(b)-Left
Click here to download Figure: Fig.5(b)-Left.eps

Fig.5(b)-Right

Fig.5(c)-Left

Click here to download Figure: Fig.5(c)-Left.eps

Fig.5(c)-Right
Click here to download Figure: Fig.5(c)-Right.eps

Fig.6(a)
Click here to download Figure: Fig.6(a).pdf

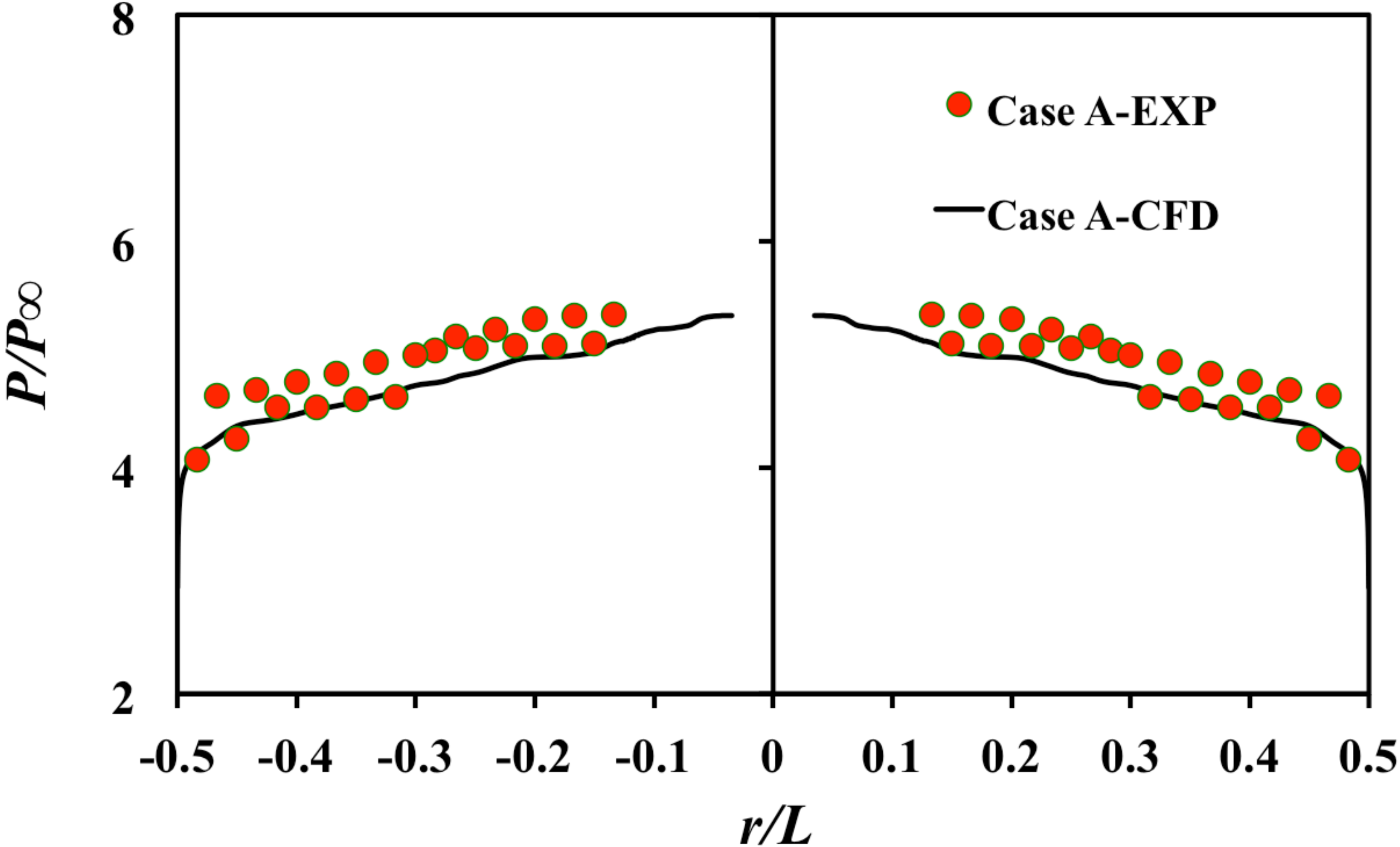

Fig.6(b)

Click here to download Figure: Fig.6(b).pdf

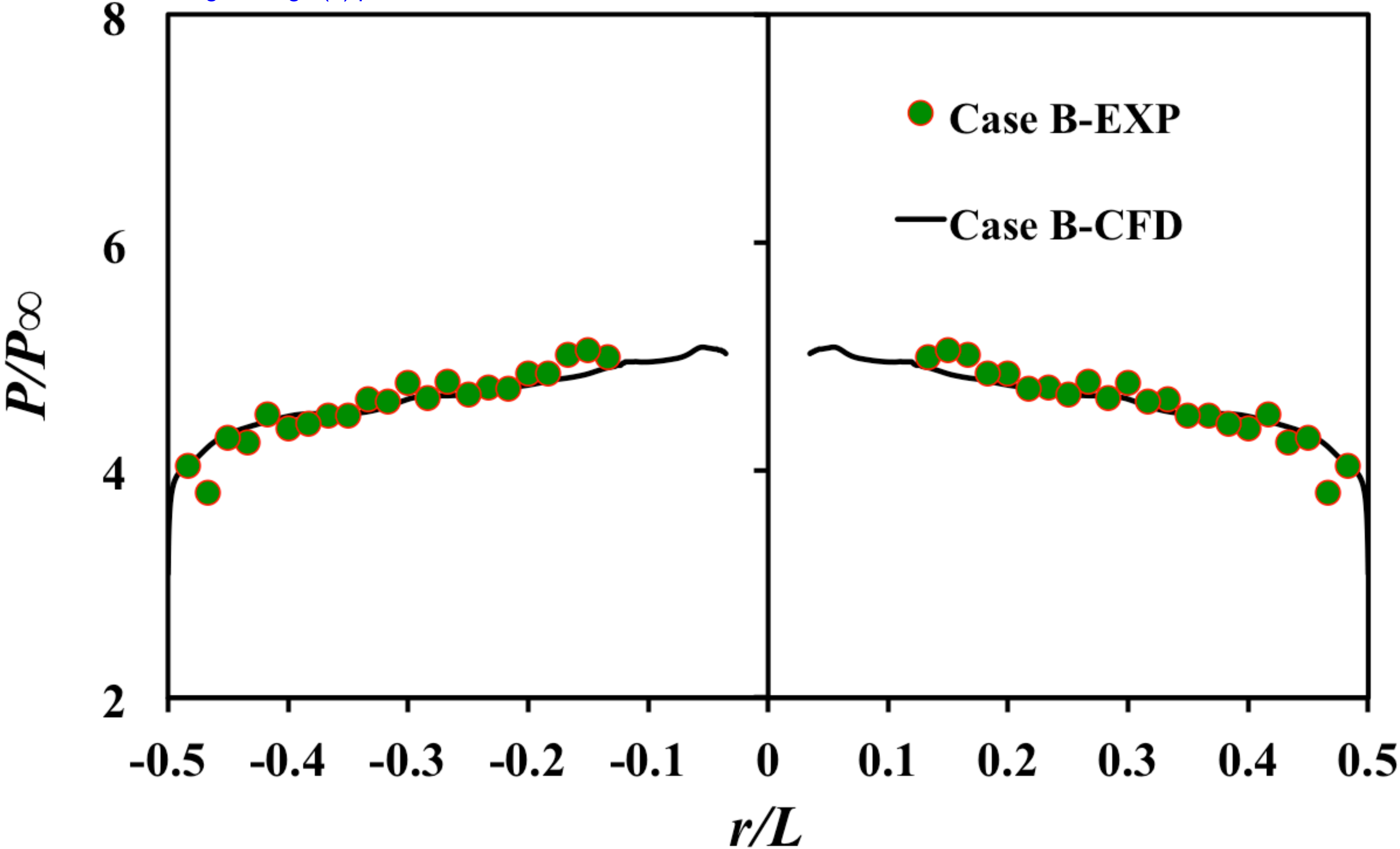

Fig.6(c)
Click here to download Figure: Fig.6(c).pdf

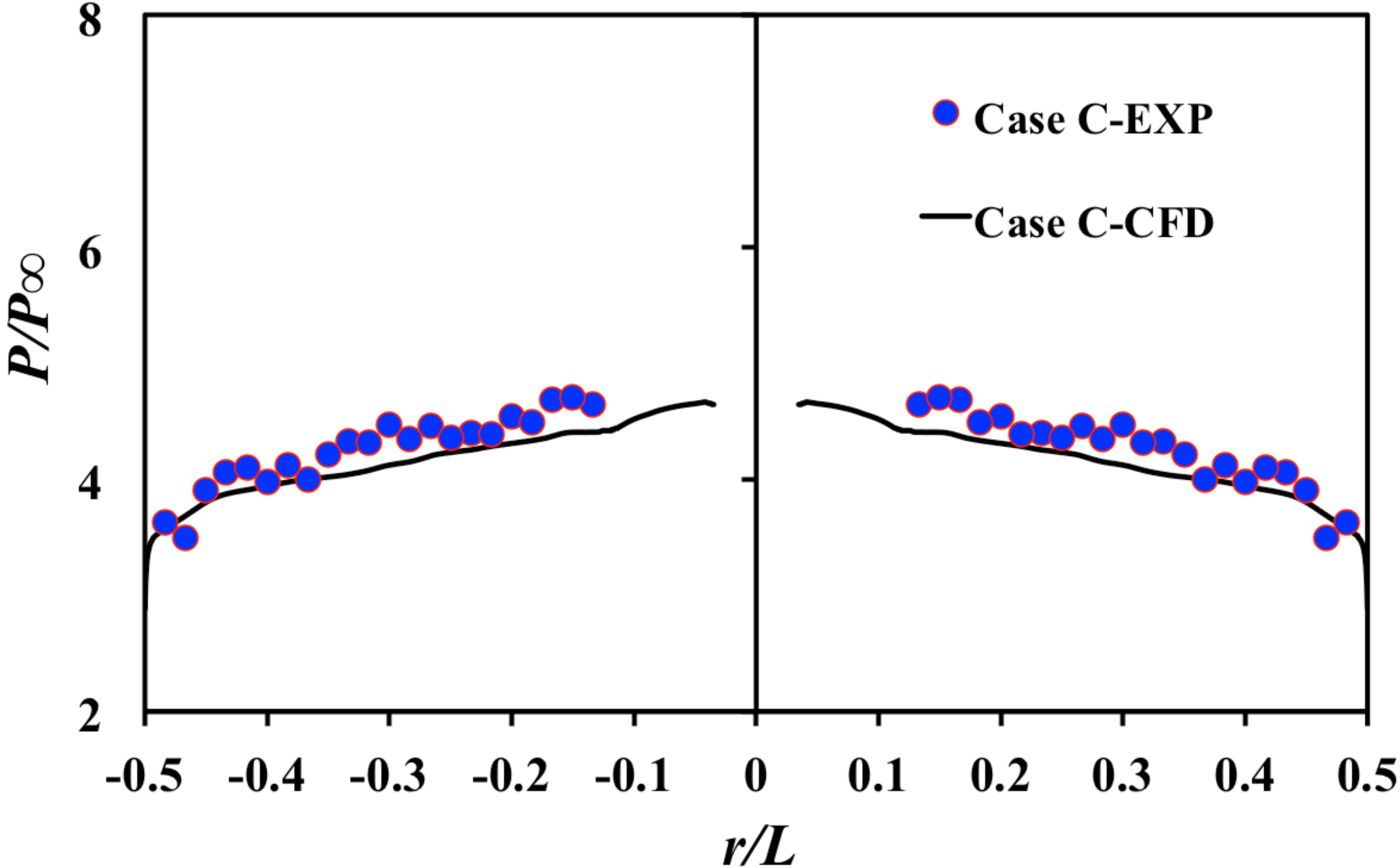

Fig. 6(d)
Click here to download Figure: Fig.6(d).pdf

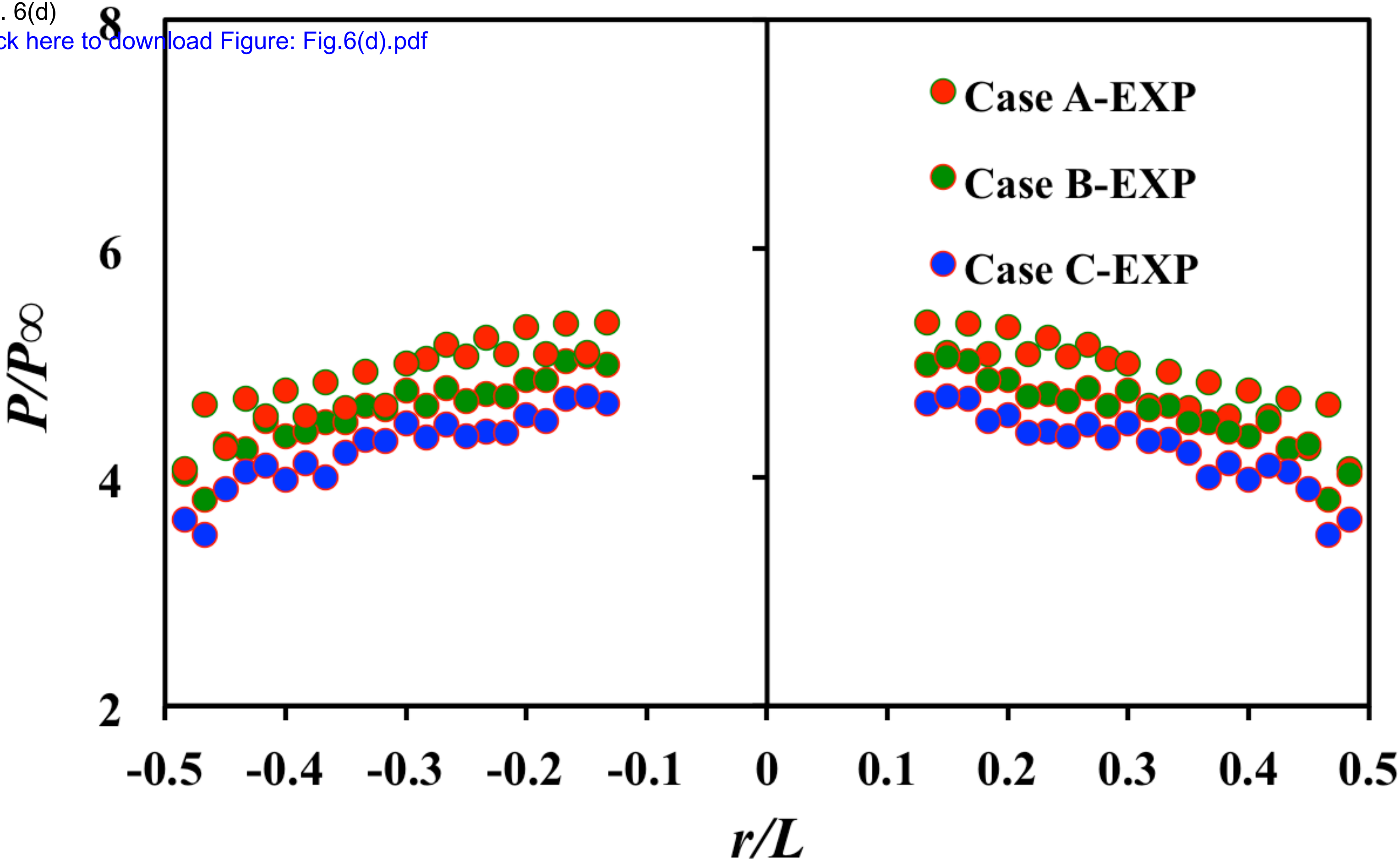

Figure Captions List

Fig. 1 (a): Parachute model used in the present computation and capsule geometry (dimensions are in the unit of mm); (b) 3D view of grid of parachute model for Case B in this study with the conditions on all the physical boundaries specified.

Fig. 1(a) No caption

Fig. 1(b) No caption

Fig. 2 Comparison of the ratios of the foreshock stand-off distance ahead of the capsule, Δ, to the distance between the capsule and the canopy, *X*=90mm, for Cases A, B and C.

Fig. 3 Comparison of experimental and CFD Strouhal numbers for the effect of the capsule half-cone angle, *θ*. The line stands for the linear fit to the Strouhal number based on the CFD pressure variation at point Q.

Fig. 4 Typical Mach number contours in two instantaneous flow fields for Cases A, B and C with increases in *θ* from 10 to 30 deg, which show the flow features of the aerodynamic interactions: the capsule wake/canopy shock and the capsule shock/canopy shock interactions. Black ellipse marks the distance between the capsule shock and canopy shocks. The same scale with a black arrow is used to compare the triple-point positions in the three cases. S1 represents the capsule shock, S2 the canopy shock, S3 and S4 the shock waves, and L1 the shear layer.

Fig. 4 (a) θ **=10 deg (left: 20/34**T_{10}**; right: 26/34**T_{10}**)**

Fig. 4 (b) θ **=20 deg (left: 19/32**T_{20}**; right: 25/32**T_{20}**)**

Fig. 4(c) θ **=30 deg (left: 17/30**T_{30}**; right: 24/30**T_{30}**)**

Fig. 5 Typical surface pressure contours in two instantaneous flow fields for Cases A, B and C with increases in *θ* from 10 to 30 deg in Fig. 4: the capsule wake/canopy shock interaction (left) and the capsule shock/canopy shock interaction (right).

Fig. 5 (a) θ **=10 deg (left: 20/34**T_{10}**; right: 26/34**T_{10}**)**

Fig. 5 (b) θ **=20 deg (left: 19/32**T_{20}**; right: 25/32**T_{20}**)**

Fig. 5(c) θ **=30 deg (left: 17/30**T_{30}**; right: 24/30**T_{30}**)**

Fig. 6 Comparison of experimental and CFD averaged pressure distribution on the inner surface of the canopy for Cases (a) A, (b) B, (c) C. (d) is a summary of the pressure distribution data for all the cases.

Fig. 6(a) No caption

Fig. 6(b) No caption

Fig. 6(c) No caption

Fig. 6(d) No caption